ADVANCED THEORY AND SIMULATIONS
www.advtheorysimul.com

Exotic Spintronic Properties of Transition-Metal Monolayers on Graphyne

*Xiaoxiong Ren, Junsheng Huang, Ping Li, Yun Zhang, and Zhi-Xin Guo**

The recent discovery of 2D magnetic materials, which are compounds of transition metals (TM) with other elements, has opened new avenues for basic research on low-dimensional magnetism and potential applications in spintronics. To further explore new 2D magnets of pure TM is an interesting topic. Based on the first-principles calculations, here a strategy of obtaining monolayer TM magnets, i.e., depositing TM atoms on graphyne (Gy), which has proper hexagonal hollow geometry, is proposed. It is found that a TM monolayer with perfect hexagonal geometry can be formed on Gy. The TM monolayer exhibits a wealth of physical properties in dependence of TM species, such as ferromagnetic and anti-ferromagnetic ground states, as well as intriguing semimetal and half-metal characteristics. It is also found that the half-metal characteristics make the monolayer TM have great potential applications in horizontal magnetic tunnel junction (MTJ) devices, where the tunneling magnetoresistance can reach as high as 850 000%. These results provide a new framework for obtaining 2D magnets with outstanding spintronic properties.

1. Introduction

2D magnetic materials can exhibit many novel physical properties, which are particularly useful in the spintronics.[1] In the past decades, magnetic 2D materials were usually created in an extrinsic way, e.g., defect engineering[2] on nonmagnetic (NM) 2D materials. Until recently, the discovery of 2D van der Waals (vdW) materials with intrinsic magnetism opens a new avenue to the 2D magnets. The interplay of dimensionality, correlation, charge, orbital character, and topology makes 2D magnetic crystals and heterostructures extremely fertile condensed matter systems with a large reservoir of exotic properties, such as quantum anomalous Hall effect,[3] unique spin–orbit coupling effect,[4] strong tunneling magnetoresistance (TMR) effect,[1d,5] and so on. These fascinating properties make them have great potential applications in the future spintronics.

At present, most studies focus on 2D magnetic materials composed of multiple compounds of transition metal (TM) and other elements, e.g., CrI_3,[6] $MnBi_2Te_4$,[7] and Fe_3GeTe_2.[8] Despite the fascinating properties of these 2D magnetic materials, the appearance of multiple element components easily induces defects such as uneven distribution of components and structures[9] during the synthesis process, which severely limits their wide application in spin-polarized devices. Therefore, it is greatly disable to find a way to obtain 2D magnetic material composed of pure TM.

On the other hand, the TM magnetic films such as Co and Fe are the mostly used magnetic materials in the present spintronic devices.[10] In order to meet the development needs of miniaturization and high performance of spintronic devices, many methods had been proposed to further reduce the thickness of TM magnetic film[11] as well as to synthesize them on a semiconductor substrate.[12] However, owing to the agglomeration nature of TM atoms and the complex surface structure of semiconductor, it is extremely hard to obtain an atomic-thick magnetic TM film on the semiconductor substrates.

2. Results and Discussion

Here we propose that the 2D magnetic material can be obtained by depositing TM atoms on graphyne (Gy), which has a hexagonal hollow geometry. The deposited TM atoms prefer to locate on the hollow site of Gy and form a perfect honeycomb monolayer. We find several TM elements such as V that are NM in their bulk phases have anti-ferromagnetic (AFM) ground state in their 2D structure, while the usually believed ferromagnetic (FM) materials such as Ni presents NM ground state. The variation of magnetism can be attributed to the combined effects of out-of-plane symmetry broken and orbital hybridization with Gy. We also find that W and Mo exhibit the 2D half-metal characteristic,

X. Ren, J. Huang, P. Li, Z.-X. Guo
State Key Laboratory for Mechanical Behavior of Materials
Center for Spintronics and Quantum System
School of Materials Science and Engineering
Xi'an Jiaotong University
Xi'an, Shaanxi 710049, China
E-mail: zxguo08@xjtu.edu.cn

Y. Zhang
Department of Physics and Information Technology
Baoji University of Arts and Sciences
Baoji 721016, China

Z.-X. Guo
Key Laboratory of Polar Materials and Devices
Ministry of Education, East China Normal University
Shanghai 200241, China

The ORCID identification number(s) for the author(s) of this article can be found under https://doi.org/10.1002/adts.202100287

DOI: 10.1002/adts.202100287

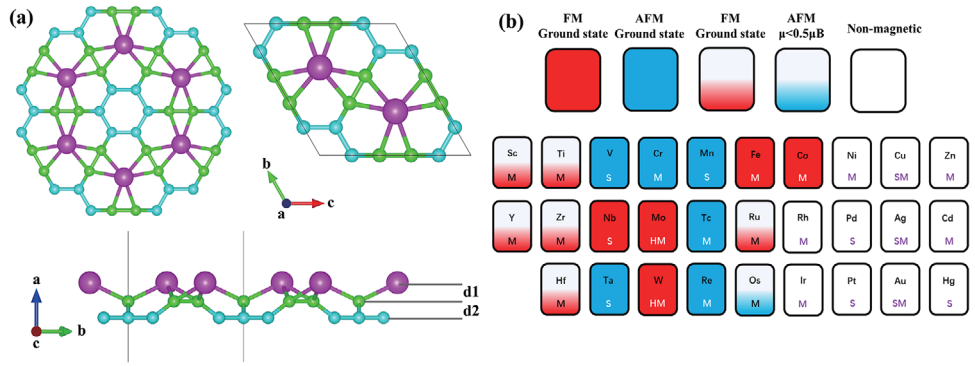

Figure 1. Calculated structure and physical characteristics of Gy/TM system. a) Hexagonal structure formed by TM in Gy/TM system (upper left), as well as the top view (upper right) and side view (lower) of a unit cell Gy/TM structure. The magenta, green, and blue atoms represent the TM atom, C atom in the nearest neighbor, and C atom in the next nearest neighbor to TM atom, respectively. d_1 and d_2 represent the distance between the TM atomic layer and the first layer C, and the distance between the two layers C, respectively. b) The physical properties of Gy/TM are given in the form of the periodic table, where the red, blue, and white background represent the magnetic ground states of ferromagnetic (FM), anti-ferromagnetic (AFM), and nonmagnetic (NM), respectively. The full and partial fillings of the background color represent that the magnetic moment of a single TM is greater than as well as less than 0.5 μ_B, respectively. The letters S, M, HM, and SM represent the properties of semiconductors, metals, half-metals, and semimetals respectively.

where the tunneling magnetoresistance in the magnetic tunnel junction (MTJ) is estimated as high as 850 000%.

We have considered γ-Gy as the substrate, which consists of hexagonal carbon rings and acetylene linkages, with six C atoms forming the $C_{sp}{\equiv}C_{sp}$ hybridization and the remaining six C atoms forming the $C_{sp^2} - C_{sp}$ hybridization, respectively.[13] Our density functional theory (DFT) calculations show that the lattice constant of freestanding Gy is 6.890 Å, agreed with previous studies.[14] We first systematically explored the stable geometries of the entire TMs from 3d to 5d on Gy. A common feature is that all the TM atoms prefer to locate on the hollow site above the center of the acetylenic ring, where the monolayer TM with graphene-like structure can be formed in a proper coverage (**Figure 1**a). Considering that the nonbonded interaction generally appears between atoms with distances of >2 times larger of their bonded length, and the nearest neighbor distances between two TM atoms are around 3.8 Å, only about 30% larger than the bond lengths in their bulk phases, it is natural to expect that there is still strong bonding interaction between them. As discussed in the following sections, this feature can lead to strong Heisenberg exchange interaction and thus the FM phase of TM monolayers. On the other hand, the strong interface interaction between the TM and C induces significant buckling of graphyne (d_1 in **Table 1**), the value of which depends on the specific TM element (highly related to the atomic radius).

To evaluate the stability, we calculated the cohesive energy E_c of monolayer TM on Gy, which is defined as[15]

$$E_c = \left(E_{Gy} + N_{TM}\mu_{TM} - E_{tot}\right)/N_{TM} \quad (1)$$

where E_{Gy} and E_{tot} are the total energies of Gy and Gy/TM, respectively, N_{TM} is the number of TM atoms on graphyne, and μ_{TM} is the chemical potential of TM which is adopted as the energy of an isolated TM atom. The cohesive energy E_c defined above is the energy gain to grow TM monolayer on the Gy surface. As shown in Table 1 and Table S1 (Supporting Information), E_c of all TM monolayers is above 2.0 eV except for five group IB and IIB elements (e.g., Ag, Au, Zn, Cd, Hg), which have completely filled orbitals. Such E_c value is larger than that of a monolayer TM on metal substrate and that of a group IV monolayer on TM substrate, both of which had been experimentally synthesized,[16] showing the possibility of experimental synthesis for the monolayer TM. Moreover, in 2014 Zhao et al.[17] had successfully trapped the Fe atoms in the pores of graphene, which finally form the single-atom-thick Fe membranes. These 2D Fe nanomembranes are directly imaged and are shown to have a square lattice at room temperature. The system in our work is similar to graphene/Fe, and the experimental growth of TM monolayer on Gy is expected to be also realized in the near future. The dynamical stability of such a system was also confirmed

Table 1. Lattice constants and structure information of selected FM and AFM systems (*a* represents the lattice constants of the systems. *M* represents the magnetic moment of a single TM in the Gy/TM systems. The d_1 and d_2 represent the distance between the transition metal atomic layer and the first layer C and the distance between the two layers C, respectively. E_c represents the cohesive energy of TM monolayer on Gy. S means semiconductor; M means metal; and HM means half-metal.).

System	*a* [Å]	*M* [μ_B TM^{-1}]	d_1 [Å]	d_2 [Å]	Bandgap [eV]	E_c [meV]	Physical properties
Gy/V	6.566	1.096	0.77	0.82	0.345	3.352	S
Gy/Nb	6.589	0.606	0.98	0.83	0.066	4.931	S
Gy/Ta	6.588	0.642	0.93	0.86	0.367	5.940	S
Gy/Cr	7.035	3.366	0.00	0.00	–	2.117	M
Gy/Mo	6.585	1.582	0.92	0.81	–	3.512	HM
Gy/W	6.552	1.456	0.89	0.85	–	4.898	HM
Gy/Mn	6.752	3.018	0.58	0.61	0.852	2.389	S
Gy/Tc	6.632	1.721	0.84	0.75	0.398	4.240	M
Gy/Re	6.586	1.521	0.84	0.80	0.135	3.992	M
Gy/Fe	6.905	2.380	0.40	0.30	–	3.379	M
Gy/Co	6.946	1.293	0.12	0.12	–	4.013	M

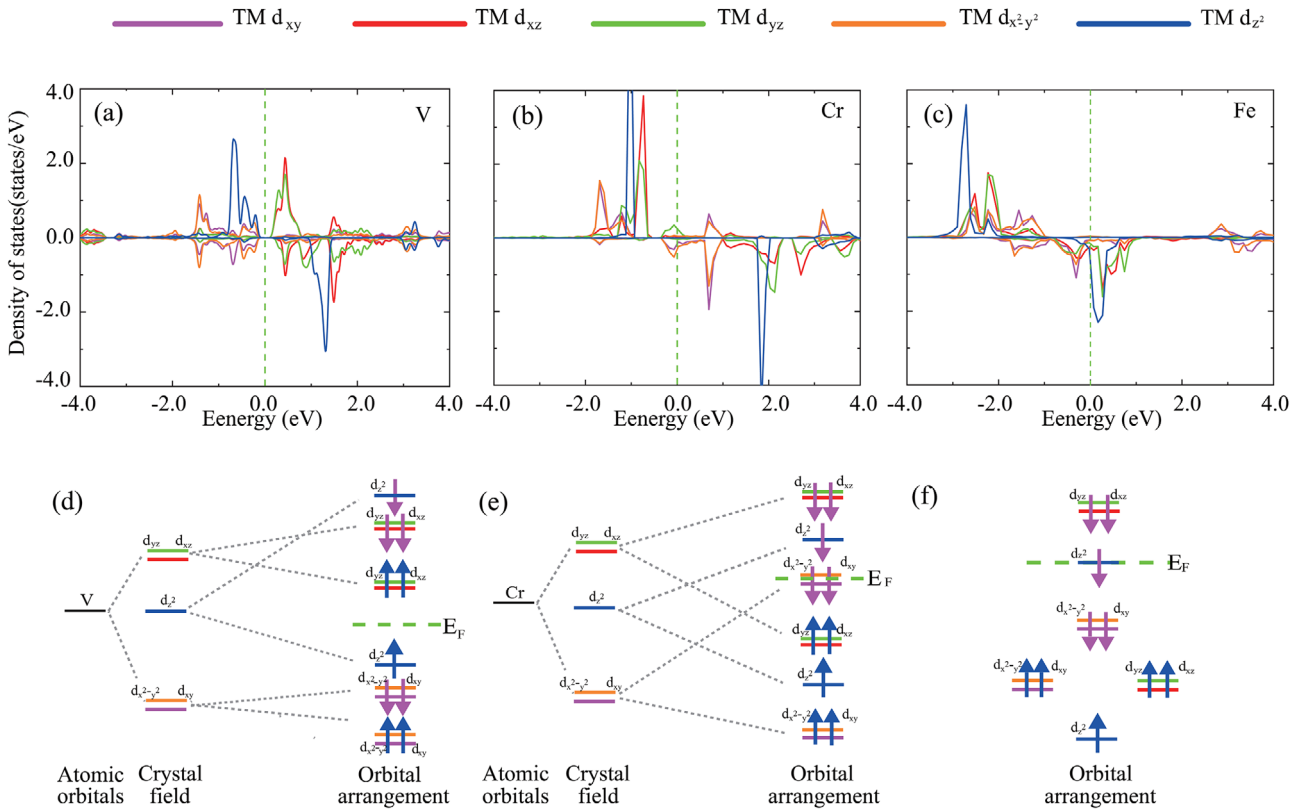

Figure 2. The calculated PDOS and d orbital arrangement of a single TM atom in the Gy/TM system. a) The d-orbital PDOS and d) orbital arrangement of a V atom in Gy/V with larger atomic radius (≥1.34 Å). The orbital arrangement characteristics for Gy/TM with TM = Cr, Mn, Te, Ta, and Re are similar to Gy/V. b,c,e,f) The results for systems with smaller atomic radius (<1.30 Å). Note that Gy/Co has similar orbital arrangement with Gy/Cr, and Gy/Mn has similar orbital arrangement with Gy/Fe. The red and green lines, the blue lines, the magenta and orange lines represent degenerate $d_{x^2-y^2}/d_{xy}$ orbitals, single d_{z^2} orbitals, and degenerated d_{xz}/d_{yz} orbitals, respectively. E_F is the Fermi level. The spilt of energy levels of d orbitals (except for Fe and Mn as discussed in the text) basically present a TPCF-like distribution.

in our previous study for Gy/Hf via ab initio molecular dynamics (AIMD) simulations.[18]

Figure 1b shows the ground states of TM monolayers on Gy in the form of an element periodic table. As one can see, TM monolayers present plentiful stable phases covering FM, AFM, and NM. Note that all the FM and AFM phases are for TM elements of group IIIB–VIIIB with partially filled d orbitals. We further define weak-FM (AFM) and strong-FM (AFM) phases for an FM (AFM) monolayer with magnetic moment smaller and larger than 0.5 μ_B atom^{-1}, respectively. In addition, we have evaluated the effect of Hubbard U on the DFT results. Considering that the value of Hubbard U depends on both the structure of the system and the types of TM atoms, and there is not available experimental result for us to fit a reliable value of U in the Gy/TM system, we simply adopted U = 2.0 eV for all the Gy/TM systems with strong FM and AFM phases. As shown in Table S2 (Supporting Information), the Hubbard U does not significantly change the magnetic moment as well as the magnetic ground state in our studied system.

As shown in Figure 1b, all the elements of groups VB–VIIB have a strong FM/AFM phase, whereas the ones of groups IIIB, IVB, and a part of group VIIIB present the weak-FM/AFM phase. It is noticed that only four of VIIIB elements have FM or AFM phase, while the remaining five present the NM phase.

In order to understand the origin of magnetism in TM monolayers, we carried out the d orbital projection density of state (PDOS) analysis on TM atoms (**Figure 2**a–c). It is found that the spilt of energy levels of d orbitals (except for Fe and Mn as discussed in the following sections) basically presents a triangular-prism-crystal-field (TPCF)-like distribution, i.e., the degenerate $d_{x^2-y^2}/d_{xy}$ orbitals, d_{z^2} orbital, and degenerate d_{xz}/d_{yz} orbitals hold the energy levels from low to high energy, respectively. The formation of such a TPCF-like distribution is a result of strong hybridization between d orbitals of TM atoms and p orbitals of the underlying C atoms as indicated in Figure S1 (Supporting Information), which significantly lowers the orbital symmetry of TM atoms compared to their bulk phases. This feature is confirmed by the calculated shortest TM–C distance (about 2.2 Å), which is comparable to the sum of the covalent atomic radii of TM and C atoms. Moreover, we find that the hybridization with p orbitals can help to fill the empty d orbitals by about two electrons per TM atom. Therefore, the variation of magnetism in the 2D structure can be owing to the strong p–d orbital hybridizations that induce significant orbital symmetry breaking and orbital filling, which are responsible for the distribution of spin-up and spin-down electrons in the crystal field. Considering that both the atomic radii and number of d electrons affecting p–d orbital hybridizations vary with the type of TM element, it is reasonable to appear

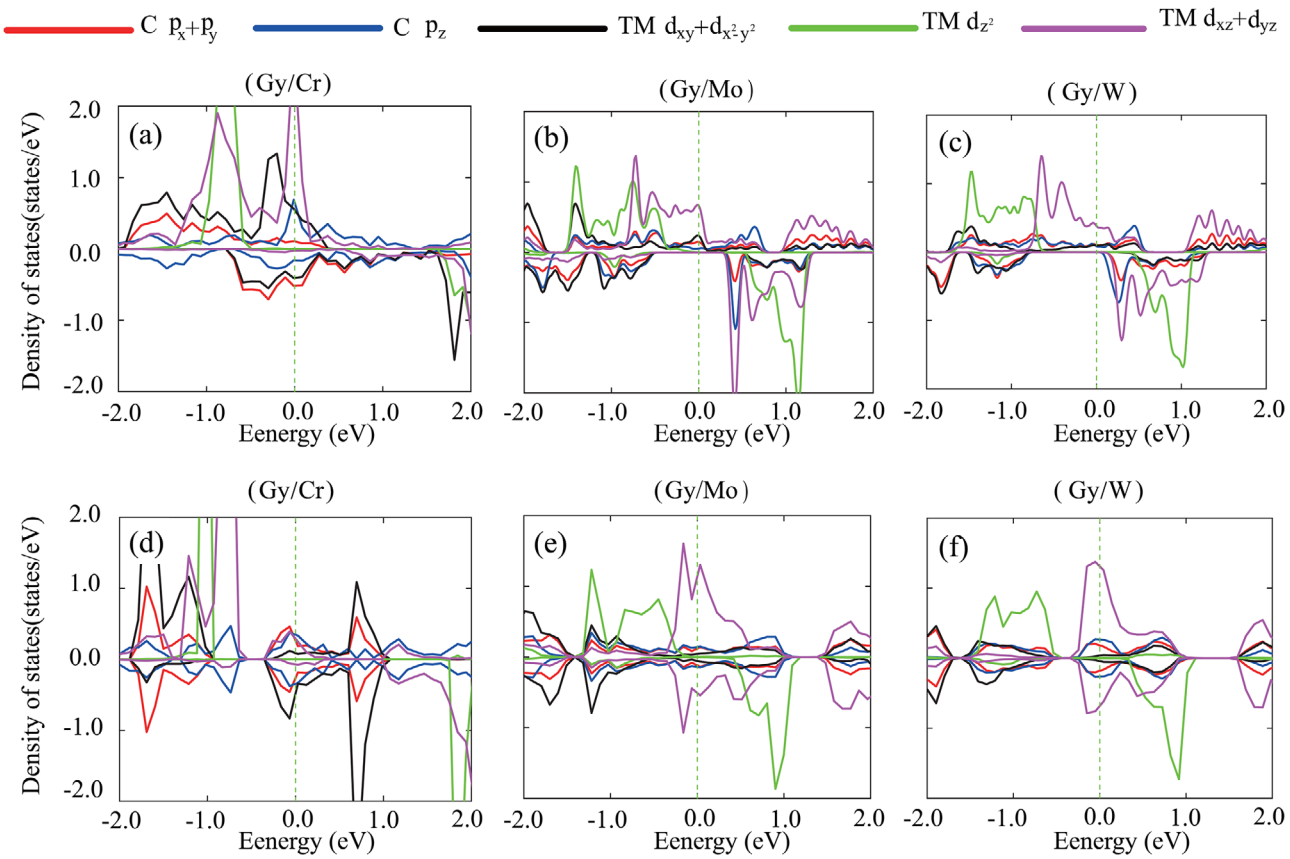

Figure 3. The calculated PDOS of Gy/TM. a–c) The PDOS of magnetic systems of Gy/TM(TM = Cr, Mo, and W). d–f) The PDOS of anti-ferromagnetic systems of them, respectively. The red (for degenerate p_x/p_y orbital) and blue (for p_z orbital) lines represent the PDOS of the six C nearest to TM, respectively. Black lines represent the degenerate $d_{x^2-y^2}/d_{xy}$ orbitals, magenta lines represent the degenerate d_{xz}/d_{yz} orbitals, and green lines represent the d_{z^2} orbitals of TM, respectively. The competition between the superexchange induced by the hybridization of p–d orbitals and the direct exchange induced by the overlaps between the d–d orbitals determines the magnetic ground state of the systems. The PDOS of d orbitals are from one TM atom of the unit cell.

of plentiful stable phases for the TM monolayers on Gy, depending not only on the group index but also on the period index. Note that, all the TM elements with six d-orbital electrons, i.e., Ni, Pd, and Pt, present the NM phase in the Gy/TM structure, because the hybridization with p orbitals of C makes s and d orbitals be completely filled.

Then we focus on the 11 TM monolayers, which have the strong FM or AFM ground states with larger magnetic momentum (>0.5 μ_B atom^{-1}). As shown in Figure 1b, 5 of 11 TM elements (e.g., Fe, Co, Nb, Mo, and W) present the strong FM ground state, and the remaining 6 TM elements (V, Cr, Mn, Te, Ta, and Re) have the strong AFM ground state. The PDOS calculations show that these ground states can be described by three kinds of orbital arrangement (Figure 2d–f). The first two are originated from the TPCF-like filed, that is, the TM elements with atomic radius larger than 1.34 Å (V, Nb, Ta, Mo, W, Tc, and Re) have d_{z^2} and d_{xz}/d_{yz} orbitals locating on the VBM and CBM, respectively, whereas those with atomic radii smaller than 1.30 Å (Cr and Co) mainly have $d_{x^2-y^2}/d_{xy}$ orbitals nearby E_F. The third kind is for Fe and Mn, which also have small atomic radii (1.26 and 1.27 Å). However, the exchange field presents complex orbital arrangement with degenerated $d_{x^2-y^2}/d_{xy}$ and d_{xz}/d_{yz} orbitals, as shown in Figure 2f, which cannot be directly derived from the TPCF-like filed. These results show that the exchange field of TM monolayer is induced by the combined effect of atomic radii (more dominating) and number of d valance electrons of the TM elements.

Based on the detailed analysis of PDOS, we found that the ground FM/AFM magnetic state is attributed to the competition between direct exchange and superexchange of d electrons. In the following, we show the details by taking Cr, Mo, and W in group VI B as an example. We first considered Cr monolayer, which has an AFM ground state. **Figure 3**a,d shows the PDOS of a Cr atom in the FM and AFM phases, respectively. It is shown that there are obvious overlaps of PDOS peaks for p_x/p_y and $d_{x^2-y^2}/d_{xy}$, as well as for p_z and d_{xz}/d_{yz} orbitals, indicating the significant p–d orbital hybridizations. Such orbital hybridizations are expected to induce strong superexchange magnetic interactions contributing to the AFM phase, between two nearest Cr atoms bridged by the two bonded C atoms (Figure 1). On the other hand, there are also direct d–d orbital overlaps between two nearest-neighbor Cr atoms, contributing to the FM phase. Therefore, the magnetic ground state is determined by the competition between the super-exchange and direct exchange effects, where the

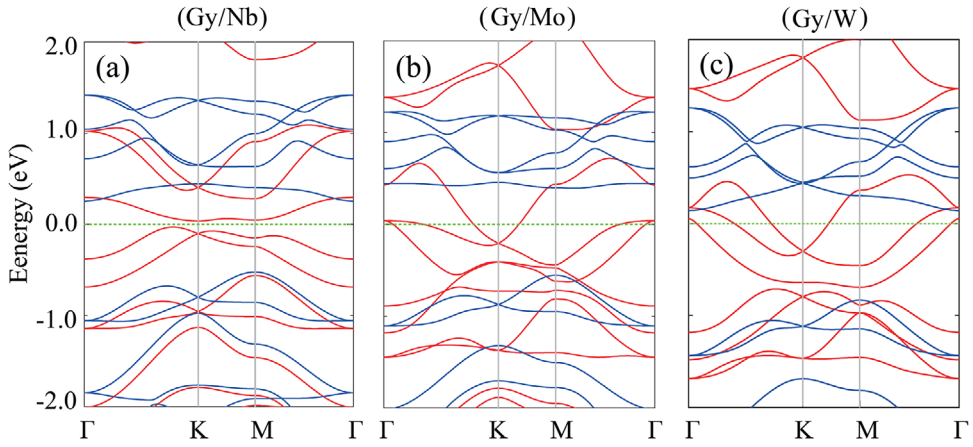

Figure 4. Half-metallic Gy/TM system. a–c) The half-metal system of Gy/TM (TM = Nb, Mo, and W). Red and blue represent the spin-up and spin-down electronic states, respectively. Gy/Nb exhibits half-semiconductor characteristic with an energy gap of 0.1 eV, where the pure spin-up electrons appear in [−0.5, 0.2] eV. Mo and W systems are half-metals with pure spin-up electrons appearing in [−0.5, 0.4] and [−0.8, 0.1] eV, respectively.

superexchange effect is dominant for Cr monolayer. Note that the direct exchange effect would be dominant for Mo and W monolayers, because the p–d orbital hybridizations contributing to the AFM phase become weaker, whereas the direct d–d orbital overlaps become stronger due to the increase of atomic radii. This feature is confirmed by the calculated PDOS of a Mo (W) atom shown in Figure 3b,e (Figure 3c,f) with both FM and AFM phases, where the overlapped peaks of p–d orbitals become obviously smaller but the width of d orbital DOS nearby Fermi level gets much larger compared to that of Cr. We have additionally calculated and analyzed the spin chare density of Gy/Cr, Gy/Mo, and Gy/W ground states (Figure S5, Supporting Information), and found that the results are consistent with the PDOS analysis.

In addition, we have calculated the exchange constant J for the Gy/TM with the magnetic moment larger than 0.5 μ_B per TM atom (Table S2, Supporting Information). It is found that the exchange constant of some structures, i.e., Gy/Mo and Gy/W, reaches around −30 meV, meaning that their Curie temperatures are at room-temperature level. To ensure this, we have further explored the Curie temperatures of Gy/Mo and Gy/W. The calculation was performed by using the Monte Carlo method, where the corresponding parameters are obtained by the DFT calculations. The calculation results are shown in Figure S4 (Supporting Information). It is found that the Curie temperatures of Gy/Mo and Gy/W are 243 and 293 K, respectively, which are pretty high in comparison with the usual 2D magnetic materials.[6,7]

Now we come to discuss the electronic properties of Gy/TM. As shown in Figure 1b and in Figure S3 (Supporting Information), the TM monolayers exhibit plentiful electronic properties, including metal, semiconductor, as well as semimetal. Particularly, the FM and AFM systems are of great interest for potential device applications, and here we focus on the TM monolayers with FM ground state. **Figure 4** shows the calculated band structures of Nb, Mo, and W monolayers on Gy, which exhibit either half-metal or half-semiconductor characteristics distinguished from their bulk phases. As shown in Figure 4, Mo and W monolayers are ideal half-metals with pure spin-up electrons appearing in [−0.5, 0.4] and [−0.8, 0.1] eV, respectively. However, Nb monolayer exhibits half-semiconductor characteristic with an energy gap of 0.1 eV, where the pure spin-up electrons appears in [−0.5, 0.2] eV. On the other hand, although the Fe and Co monolayers do not have half-metal characteristics, they still have pure spin-down electrons nearby the Fermi level, i.e., [−1.0, −0.2] and [−0.7, −0.3] eV, respectively (Figure S2, Supporting Information). This feature shows that these TM monolayers can be ideal materials for the spin-transport devices.

To verify the application potentials of TM monolayers in the spintronic devices, we further explored the TMR of a horizontal MTJ device based on the Gy/TM structure (**Figure 5**a). It is known that the vertical MTJ devices based on 2D materials have been widely studied in the past decade; however, the investigation on horizontal MTJ is still scarce due to the difficulty in realizing the 2D horizontal magnetic heterostructures in experiments. Here we propose that one can realize the horizontal MTJ device much easier in the use of the Gy/TM system, i.e., deposit different TM atoms using the mask method to make magnetic layers, and leave undeposited region (bare Gy) as the tunneling layer. Note that the bare Gy is a semiconductor with a bandgap of about 0.4 eV, which makes the undeposited Gy region an ideal candidate for the tunneling layer.[19]

We further show a horizontal MTJ device model in Figure 5a, where the source and drain electrodes are composed of Gy/Mo, and the free magnetic layer and tunneling layer are composed by Gy/W and bare Gy, respectively. The parallel (P) and antiparallel (AP) magnetization states of the MTJ are realized by flipping the magnetization direction of W monolayer as indicated in Figure 5b. The calculated transmission spectra of the P and AP states for different spins with zero bias are shown in Figure 5c. As one can see, in both cases the spin-up ($T_\uparrow$) electron transmission is larger than that of spin-down ($T_\downarrow$) electrons nearby the Fermi level by about ten orders, manifesting a perfect spin-filtering effect. We further evaluated the TMR of the MTJ, which is defined as $|(T_P - T_{AP})/T_{AP}| \times 100\%$, with $T_P = T_\uparrow + T_\downarrow$ and $T_{AP} = T_\uparrow + T_\downarrow$, respectively. As shown in Figure 5d, the 2D device has exceptionally TMR of about 2800% at the Fermi level and 850 000% at −0.63 eV, respectively. Especially, the 850 000% is significantly larger than the reported record realized in the vertical MTJ based on multilayer CrI_3 (57 000%).[20]

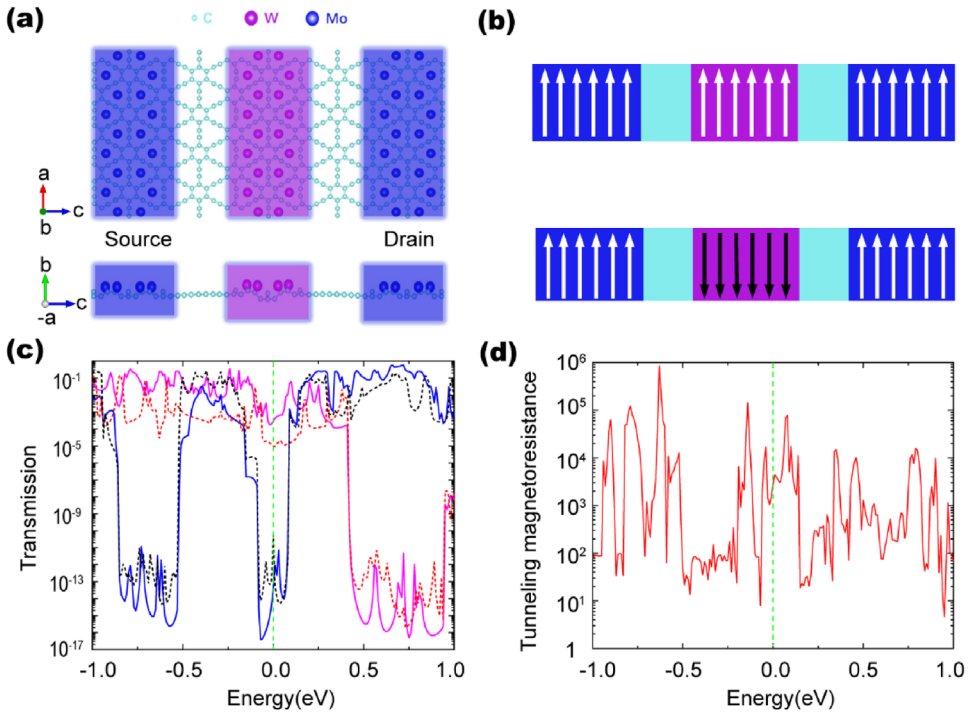

Figure 5. Gy/TM horizontal MTJ device model and calculated electronic transport properties. a) MTJ device model in top view (upper panel) and side view (lower panel). b) Schematic diagram of the magnetic sequence of the device changing from a parallel (P) state to an antiparallel (AP) state. c) Calculated transmission spectra of the P and AP states under zero bias. The solid and the dashed line represent the device configuration in the P and AP states, respectively. The magenta (red) and blue (black) solid lines represent the transmission for spin-up and spin-down states, respectively. d) Calculated tunneling magnetoresistance as a function of energy level.

The unusually high TMR can be attributed to the half-metal properties of Gy/W and Gy/Mo, which induce much larger transmission probability of spin-up electrons than that of the spin-down electrons in Gy/W, with the Gy/Mo region being in the spin-up state (Figure 5b,c). Due to the spin-transfer torque effect, the transmission probability of majority spins in the P state is several orders of magnitude higher than at of AP state, which results in the high TMR for the MTJ. We have also explored the *I*–*V* curve (Figure S7, Supporting Information). It is found that the current density of them under 0.1 V is obviously larger than that in the vertical MTJ based of multilayer CrI_3.[20] This result indicates that the horizontal Gy/TM-type MTJ is more superior to the low-power spintronic devices.

3. Conclusion

In summary, by using the first-principles calculations, we have proposed a new approach to obtain monolayer TM magnets, i.e., depositing TM atoms on substrate with hexagonal hollow geometry. We have demonstrated the feasibility of this approach on Gy substrate, where the TM monolayer with perfect hexagonal geometry has been formed. We have also found that the TM monolayer exhibits a wealth of physical properties, including FM and AFM ground states, as well as semimetal and half-metal characteristics. The competition between direct exchange and superexchange interactions has been proposed to explain the variation of magnetic phases. Finally, we have demonstrated that the TM monolayers have great potential applications in the spintronics, where the TMR in the horizontal MTJ device model is calculated to be 2800% at the Fermi level and as high as 850 000% at −0.63 eV, respectively.

4. Experimental Section

The first-principles calculations were performed by using the DFT-based Vienna ab initio simulation package (VASP).[21] The ion–electron interaction was treated by the projector augmented-wave (PAW) technique.[22] Exchange–correlation energies were taken into account by the generalized gradient approximation (GGA) using the Perdew–Burke–Ernzerhof (PBE) functional.[23] For TM monolayer, periodic boundary condition for the 2D structure was used, and a vacuum layer of 15 Å was set to avoid interactions in the out-of-plane direction. A plane-wave basis set with a cutoff energy of 450 eV was used, and the first Brillouin-zone integration was carried out by a 15 × 15 × 1 Γ-centered Monkhorst–Pack grid.[24] Both of the atomic positions and lattice constants were optimized using a conjugate gradient method with criteria of energy and Hellmann–Feynman force convergence being $<10^{-6}$ eV per unit cell and 0.01 eV $Å^{-1}$, respectively.

As for the calculation of tunneling magnetoresistance in the MTJ, the atomic positions were optimized using a conjugate gradient method with criteria of energy and Hellmann–Feynman force convergence being less than 10^{-5} eV per unit cell and 0.02 eV $Å^{-1}$, respectively. Then the MTJ device model was constructed, as shown in Figure 4a. The transmission calculations were carried out using the Atomistic Simulation Toolkit (ATK) with the PBE pseudopotentials distributed in the QuantumWise package.[25] The transmission was calculated using the nonequilibrium Green's function (NEGF) approach.[26] A Gy/W/Gy supercell was used as the scattering region, ideally attached on both sides to semi-infinite Gy/Mo leads.[27] The Dirichlet boundary condition in the *c*-direction and

periodic boundary conditions in the *a*–*b* plane were used in the simulation (Figure 4a), and the length of electrodes was 6.712 Å. The temperature was set at 300 K. The convergence tested (Figure S6, Supporting Information) Monkhorst–Pack grid (15 × 1 × 100) was used with a mesh cutoff energy (55 Hartree) for the electrodes and central region. The medium basis set was adopted with PseudoDojo pseudopotentials. The NEGF–DFT self-consistency was controlled by a numerical tolerance of 10^{-5} eV.

Supporting Information

Supporting Information is available from the Wiley Online Library or from the author.

Acknowledgements

The authors are grateful for useful discussions with Dr. Lei Wang and Dr. Yongliang Shi. This work was supported by the National Key R&D Program of China (Program No. 2018YFB0407600), National Natural Science Foundation of China (Grant Nos. 12074301 and 12004295), Science Fund for Distinguished Young Scholars of Hunan Province (Grant No.2018JJ1022), Fundamental Research Funds for Central Universities (Grant No. xzy012019062), and Open Research Fund of Key Laboratory of Polar Materials and Devices, Ministry of Education. P.L. thanks China's Postdoctoral Science Foundation funded project (Project No. 2020M673364).

Conflict of Interest

The authors declare no conflict of interest.

Data Availability Statement

Research data are not shared.

Keywords

half-metals, horizontal magnetic tunnel junctions, magnetic monolayer films, transition metals

Received: August 4, 2021
Revised: September 19, 2021
Published online:

[1] a) Z. Wang, D. K. Ki, H. Chen, H. Berger, A. H. MacDonald, A. F. Morpurgo, *Nat. Commun.* **2015**, *6*, 8339; b) W. Han, *APL Mater.* **2016**, *4*, 032401; c) Y. P. Feng, L. Shen, M. Yang, A. Wang, M. Zeng, Q. Wu, S. Chintalapati, C. R. Chang, *Wiley Interdiscip. Rev.: Comput. Mol. Sci.* **2017**, *7*, e1313; d) H. H. Kim, B. Yang, T. Patel, F. Sfigakis, C. Li, S. Tian, H. Lei, A. W. Tsen, *Nano Lett.* **2018**, *18*, 4885; e) Q. Xie, W. Lin, B. Yang, X. Shu, S. Chen, L. Liu, X. Yu, M. B. Breese, T. Zhou, M. Yang, *Adv. Mater.* **2019**, *31*, 1900776.

[2] a) O. V. Yazyev, L. Helm, *Phys. Rev. B* **2007**, *75*, 125408; b) R. Nair, M. Sepioni, I.-L. Tsai, O. Lehtinen, J. Keinonen, A. Krasheninnikov, T. Thomson, A. Geim, I. Grigorieva, *Nat. Phys.* **2012**, *8*, 199; c) W. Han, R. K. Kawakami, M. Gmitra, J. Fabian, *Nat. Nanotechnol.* **2014**, *9*, 794; d) J. Červenka, M. Katsnelson, C. Flipse, *Nat. Phys.* **2009**, *5*, 840; e) K. M. McCreary, A. G. Swartz, W. Han, J. Fabian, R. K. Kawakami, *Phys. Rev. Lett.* **2012**, *109*, 186604; f) A. Giesbers, K. Uhlířová, M. Konečný, E. Peters, M. Burghard, J. Aarts, C. Flipse, *Phys. Rev. Lett.* **2013**, *111*, 166101; g) D. Boukhvalov, M. Katsnelson, A. Lichtenstein, *Phys. Rev. B* **2008**, *77*, 035427; h) O. V. Yazyev, M. Katsnelson, *Phys. Rev. Lett.* **2008**, *100*, 047209; i) J. Jung, T. Pereg-Barnea, A. MacDonald, *Phys. Rev. Lett.* **2009**, *102*, 227205; j) Y.-W. Son, M. L. Cohen, S. G. Louie, *Nature* **2006**, *444*, 347; k) T. Stauber, N. Peres, F. Guinea, A. C. Neto, *Phys. Rev. B* **2007**, *75*, 115425; l) E. V. Castro, N. Peres, T. Stauber, N. Silva, *Phys. Rev. Lett.* **2008**, *100*, 186803.

[3] a) D. Maryenko, A. Mishchenko, M. Bahramy, A. Ernst, J. Falson, Y. Kozuka, A. Tsukazaki, N. Nagaosa, M. Kawasaki, *Nat. Commun.* **2017**, *8*, 14777; b) Y. Deng, Y. Yu, Y. Song, J. Zhang, N. Z. Wang, Z. Sun, Y. Yi, Y. Z. Wu, S. Wu, J. Zhu, *Nature* **2018**, *563*, 94; c) P. Li, Y. Ma, Y. Zhang, Z.-X. Guo, *ACS Appl. Electron. Mater.* **2021**, *3*, 1826; d) P. Li, T.-Y. Cai, *Phys. Chem. Chem. Phys.* **2020**, *22*, 549.

[4] a) S. Parkin, N. More, K. Roche, *Phys. Rev. Lett.* **1990**, *64*, 2304; b) J. L. Lado, J. Fernández-Rossier, *2D Mater.* **2017**, *4*, 035002.

[5] G. Binasch, P. Grünberg, F. Saurenbach, W. Zinn, *Phys. Rev. B* **1989**, *39*, 4828.

[6] B. Huang, G. Clark, E. Navarro-Moratalla, D. R. Klein, R. Cheng, K. L. Seyler, D. Zhong, E. Schmidgall, M. A. McGuire, D. H. Cobden, *Nature* **2017**, *546*, 270.

[7] J. Li, Y. Li, S. Du, Z. Wang, B.-L. Gu, S.-C. Zhang, K. He, W. Duan, Y. Xu, *Sci. Adv.* **2019**, *5*, eaaw5685.

[8] M. M. Otrokov, I. I. Klimovskikh, H. Bentmann, A. Zeugner, Z. S. Aliev, S. Gass, A. U. Wolter, A. V. Koroleva, D. Estyunin, A. M. Shikin, *Nature* **2019**, *576*, 416.

[9] a) C. Gong, L. Li, Z. Li, H. Ji, A. Stern, Y. Xia, T. Cao, W. Bao, C. Wang, Y. Wang, *Nature* **2017**, *546*, 265; b) W. Zhou, X. Zou, S. Najmaei, Z. Liu, Y. Shi, J. Kong, J. Lou, P. M. Ajayan, B. I. Yakobson, J.-C. Idrobo, *Nano Lett.* **2013**, *13*, 2615; c) F. Banhart, J. Kotakoski, A. V. Krasheninnikov, *ACS Nano* **2011**, *5*, 26; d) Z. Lin, A. McCreary, N. Briggs, S. Subramanian, K. Zhang, Y. Sun, X. Li, N. J. Borys, H. Yuan, S. K. Fullerton-Shirey, *2D Mater.* **2016**, *3*, 042001.

[10] a) Y. J. Zheng, Y. Chen, Y. L. Huang, P. K. Gogoi, M.-Y. Li, L.-J. Li, P. E. Trevisanutto, Q. Wang, S. J. Pennycook, A. T. Wee, *ACS Nano* **2019**, *13*, 6050; b) S. Ikeda, J. Hayakawa, Y. M. Lee, F. Matsukura, Y. Ohno, T. Hanyu, H. Ohno, *IEEE Trans. Electron Devices* **2007**, *54*, 991; c) K. Sato, H. Katayama-Yoshida, *Semicond. Sci. Technol.* **2002**, *17*, 367.

[11] a) S. Ghosh, C. Choubey, A. Sil, *Superlattices Microstruct.* **2019**, *125*, 271; b) C. Xu, L. Wang, Z. Liu, L. Chen, J. Guo, N. Kang, X.-L. Ma, H.-M. Cheng, W. Ren, *Nat. Mater.* **2015**, *14*, 1135; c) K. S. Novoselov, A. K. Geim, S. V. Morozov, D. Jiang, Y. Zhang, S. V. Dubonos, I. V. Grigorieva, A. A. Firsov, *Science* **2004**, *306*, 666.

[12] a) L. Verger, C. Xu, V. Natu, H.-M. Cheng, W. Ren, M. W. Barsoum, *Curr. Opin. Solid State Mater. Sci.* **2019**, *23*, 149; b) Y. V. Goryunov, N. Garif'yanov, G. Khaliullin, I. Garifullin, L. Tagirov, F. Schreiber, T. Mühge, H. Zabel, *Phys. Rev. B* **1995**, *52*, 13450; c) Y. Xu, E. Kernohan, D. Freeland, A. Ercole, M. Tselepi, J. Bland, *Phys. Rev. B* **1998**, *58*, 890.

[13] a) Q. Li, Y. Li, Y. Chen, L. Wu, C. Yang, X. Cui, *Carbon* **2018**, *136*, 248; b) J. Kang, J. Li, F. Wu, S.-S. Li, J.-B. Xia, *J. Phys. Chem. C* **2011**, *115*, 20466; c) L. Pan, L. Zhang, B. Song, S. Du, H.-J. Gao, *Appl. Phys. Lett.* **2011**, *98*, 173102; d) N. Narita, S. Nagai, S. Suzuki, K. Nakao, *Phys. Rev. B* **1998**, *58*, 11009.

[14] a) G. Li, Y. Li, H. Liu, Y. Guo, Y. Li, D. Zhu, *Chem. Commun.* **2010**, *46*, 3256; b) Y. Jiao, A. Du, M. Hankel, Z. Zhu, V. Rudolph, S. C. Smith, *Chem. Commun.* **2011**, *47*, 11843; c) K. Srinivasu, S. K. Ghosh, *J. Phys. Chem. C* **2012**, *116*, 5951; d) J. He, P. Zhou, N. Jiao, S. Ma, K. Zhang, R. Wang, L. Sun, *Sci. Rep.* **2015**, *4*, 4014; e) S. Kim, A. R. Puigdollers, P. Gamallo, F. Vines, J. Y. Lee, *Carbon* **2017**, *120*, 63; f) S. Jana, S. Chowdhury, D. Jana, A. Chakrabarti, A. Banerjee, *J. Phys.: Condens. Matter* **2021**, *33*, 205501; g) L. Pan, B. Song, J. Sun, L. Zhang, W. Hofer, S. Du, H.-j. Gao, *J. Phys.: Condens. Matter* **2013**, *25*, 505502.

[15] P. Li, X. Li, W. Zhao, H. Chen, M.-X. Chen, Z.-X. Guo, J. Feng, X.-G. Gong, A. H. MacDonald, *Nano Lett.* **2017**, *17*, 6195.

[16] a) L. Li, Y. Wang, S. Xie, X.-B. Li, Y.-Q. Wang, R. Wu, H. Sun, S. Zhang, H.-J. Gao, *Nano Lett.* **2013**, *13*, 4671; b) J. Zhao, H. Liu, Z. Yu, R. Quhe, S. Zhou, Y. Wang, C. C. Liu, H. Zhong, N. Han, J. Lu, *Prog. Mater. Sci.* **2016**, *83*, 24; c) H. Oughaddou, H. Enriquez, M. R. Tchalala, H. Yildirim, A. J. Mayne, A. Bendounan, G. Dujardin, M. A. Ali, A. Kara, *Prog. Surf. Sci.* **2015**, *90*, 46.
[17] J. Zhao, Q. Deng, A. Bachmatiuk, G. Sandeep, A. Popov, J. Eckert, M. H. Rümmeli, *Science* **2014**, *343*, 1228.
[18] K. Wang, Y. Zhang, W. Zhao, P. Li, J.-W. Ding, G.-F. Xie, Z.-X. Guo, *Phys. Chem. Chem. Phys.* **2019**, *21*, 9310.
[19] A. R. Puigdollers, G. Alonso, P. Gamallo, *Carbon* **2016**, *96*, 879.
[20] T. Song, M. W.-Y. Tu, C. Carnahan, X. Cai, T. Taniguchi, K. Watanabe, M. A. McGuire, D. H. Cobden, D. Xiao, W. Yao, *Nano Lett.* **2019**, *19*, 915.
[21] a) G. Kresse, J. Furthmüller, *Phys. Rev. B* **1996**, *54*, 11169; b) G. Kresse, J. Hafner, *Phys. Rev. B* **1993**, *47*, 558.
[22] a) G. Kresse, D. Joubert, *Phys. Rev. B* **1999**, *59*, 1758; b) P. E. Blöchl, *Phys. Rev. B* **1994**, *50*, 17953.
[23] H. J. Monkhorst, J. D. Pack, *Phys. Rev. B* **1976**, *13*, 5188.
[24] L. Jelver, P. M. Larsen, D. Stradi, K. Stokbro, K. W. Jacobsen, *Phys. Rev. B* **2017**, *96*, 085306.
[25] a) M. Brandbyge, J.-L. Mozos, P. Ordejón, J. Taylor, K. Stokbro, *Phys. Rev. B* **2002**, *65*, 165401; b) J. M. Soler, E. Artacho, J. D. Gale, A. García, J. Junquera, P. Ordejón, D. Sánchez-Portal, *J. Phys.: Condens. Matter* **2002**, *14*, 2745.
[26] J. Taylor, H. Guo, J. Wang, *Phys. Rev. B* **2001**, *63*, 245407.
[27] a) S. Grimme, J. Antony, S. Ehrlich, H. Krieg, *J. Chem. Phys.* **2010**, *132*, 154104; b) S. Grimme, S. Ehrlich, L. Goerigk, *J. Comput. Chem.* **2011**, *32*, 1456.